Protein Engineering, Design & Selection, 2017, vol. 30 no. 3, pp. 191–198
doi: 10.1093/protein/gzw073
Advance Access Publication Date: 10 January 2017
Original Article

Original Article

Modification of the peroxygenative: peroxidative activity ratio in the unspecific peroxygenase from *Agrocybe aegerita* by structure-guided evolution

Diana M. Mate†, Miguel A. Palomino†, Patricia Molina-Espeja†, Javier Martin-Diaz, and Miguel Alcalde*

Department of Biocatalysis, Institute of Catalysis, CSIC, Marie Curie 2, 28049 Madrid, Spain

*To whom correspondence should be addressed. E-mail: malcalde@icp.csic.es.
†These authors contributed equally to the work.
Edited By Rik Wierenga

Received 14 October 2016; Revised 24 November 2016; Editorial Decision 29 November 2016; Accepted 12 December 2016

Abstract

Unspecific peroxygenase (UPO) is a heme-thiolate peroxidase capable of performing with high-selectivity C–H oxyfunctionalizations of great interest in organic synthesis through its peroxygenative activity. However, the convergence of such activity with an unwanted peroxidative activity encumbers practical applications. In this study, we have modified the peroxygenative:peroxidative activity ratio (P:p ratio) of UPO from *Agrocybe aegerita* by structure-guided evolution. Several flexible loops (Glu1-Pro35, Gly103-Asp131, Ser226-Gly243, Gln254-Thr276 and Ty293-Arg327) were selected on the basis on their *B*-factors and $\Delta\Delta G$ values. The full ensemble of segments (43% of UPO sequence) was subjected to focused evolution by the *Mutagenic Organized Recombination Process by Homologous IN vivo Grouping* (MORPHING) method in *Saccharomyces cerevisiae*. Five independent mutant libraries were screened in terms of P:p ratio and thermostability. We identified several variants that harbored substitutions at positions 120 and 320 with a strong enhancement in the P:p ratio albeit at the cost of stability. The most thermostable mutant of this process (S226G with an increased T_{50} of 2°C) was subjected to further combinatorial saturation mutagenesis on Thr120 and Thr320 yielding a collection of variants with modified P:p ratio and recovered stability. Our results seem to indicate the coexistence of several oxidation sites for peroxidative and peroxygenative activities in UPO.

Key words: peroxidative activity, peroxygenative activity, structure-guided evolution, thermostability, unspecific peroxygenase

INTRODUCTION

During the past three decades, the scientific community has compiled an impressive amount of knowledge on the function, structure and mechanism of different enzymes while engineering them to work in different biotechnological settings (Molina-Espeja *et al.*, 2016a). Particularly, the implementation of enzymes in industrial processes mostly relies on improving their stability and activity by directed evolution. To save screening efforts, current trends in evolving protein function are frequently supported by available structural information along with the appropriate use of computational algorithms such that specific regions or catalytic relevant residues can be unveiled (Verma *et al.*, 2012; Damborsky and Brezovsky, 2014). More specifically, amino acids at flexible loops that connect secondary motifs are thought to be suitable targets for mutagenesis since they typically show lower interactions than internal counterparts so that their modification can improve the protein robustness through establishing

new intramolecular contacts (Nestl and Hauer, 2014). Besides, in such regions, we can also identify valuable hotspots involved in catalysis as it is the case of many ligninolytic peroxidases that can perform complex oxidations through long-range electron transfer (LRET) pathways from the protein surface to the buried heme domain (Ruiz-Dueñas *et al.*, 2009).

The unspecific peroxygenase (UPO; EC 1.11.2.1) represents the first true self-sufficient natural peroxygenase. Discovered over one decade ago in the edible basidiomycete *Agrocybe aegerita*, this enzyme is capable of performing with high-selectivity C–H oxyfunctionalizations of great significance triggered only by H_2O_2 that works both as oxygen donor and final electron acceptor (Ullrich *et al.*, 2004; Hofrichter and Ullrich, 2006; Hofrichter *et al.*, 2010). Recently, UPO was recognized as a member of the heme-thiolate protein superfamily (together with cytochrome P450 monooxygenases and the chloroperoxidase from *Caldariomyces fumago*-CPO) (Hofrichter *et al.*, 2015). While over 1000 UPO-like genes have been mined from genomic databases, only three UPOs have been hitherto biochemically characterized (from *Coprinellus radians*, *Marasmius rotula* and *A. aegerita*). In particular, the UPO from *A. aegerita* (*Aae*UPO1) has been studied in depth in many complex oxygen-transfer reactions while it has been recently expressed in heterologous hosts and its crystal structure solved (Hofrichter and Ullrich, 2013; Molina-Espeja *et al.*, 2014, 2015; Piontek *et al.*, 2013). The *Aae*UPO1 is a 46 kDa extracellular glycoprotein formed by 10 α-helices and 5 short β-sheets. The axial ligand of the heme domain is a cysteine residue which is supposed to be determinant for the oxygen-transfer—peroxygenative—activity. Substrates access to the heme through a hydrophobic channel, with two phenylalanines delimiting the entrance to the pocket and three more involved in positioning the substrate whereas the coexistence of other catalytic sites (by LRET) is currently under investigation (Molina-Espeja *et al.*, 2016b).

Indeed, all UPO known show both peroxidative and peroxygenative activities. The latter is of particular relevance since it allows the enzyme to make aromatic and aliphatic hydroxylations, aromatic and aliphatic epoxidation, sulfoxidations, N-oxidations, N-dealkylation, bromination or ether cleavage (Hofrichter *et al.*, 2010; Hofrichter and Ullrich, 2013). Despite its biotechnological potential, the convergence of peroxidative and peroxygenative activities within the same enzyme becomes problematic. Since the product released by the peroxygenative activity—especially in the case of aromatic hydroxylation—can be substrate of the peroxidative activity, UPO oxygenation products can appear mixed with oxidation byproducts, which tend to polymerize, affecting the overall reaction yields (Fig. S1) (Molina-Espeja *et al.*, 2016b).

In this study, we have pursued to maintain/improve the peroxygenative activity while reducing the undesired peroxidative activity of UPO. As departure point, we used a recently evolved *Aae*UPO1 variant, whose expression was risen from barely undetectable levels up to 8 mg/l in *Saccharomyces cerevisiae* and over 0.2 g/l in *Pichia pastoris* (Molina-Espeja *et al.*, 2014, 2015). We first combined computational analysis (through the calculation of the *B*-factors and the ΔΔ*G* values) with a new mutagenic method for focused directed evolution based on the *S. cerevisiae* device (*Mutagenic Organized Recombination Process by Homologous IN vivo Grouping* (MORPHING)) (Gonzalez-Perez *et al.*, 2014). Five mutant libraries were constructed and screened with the goal of improving the peroxygenative:peroxidative activity ratio (P:p ratio) and the thermostability. The best mutations of this process were further studied by combinatorial saturation mutagenesis (CSM) giving rise to new variants that were characterized biochemically and their properties discussed within a structural context.

Materials and methods

Reagents and culture media

The *Aae*UPO1 secretion mutant (PaDa-I) was obtained as described elsewhere (Molina-Espeja *et al.*, 2014, 2015). Expression shuttle vector pJRoC30 came from California Institute of Technology (Pasadena, CA, USA) containing *ura*3 gene and ampicillin markers for selection. 2,2′-azino-bis-(3-ethylbenzothiazoline-6-sulfonic acid) (ABTS), 2,6-dimethoxyphenol (DMP), veratryl alcohol, *Taq* DNA polymerase and Yeast transformation kit were purchased from Sigma-Aldrich (Madrid, Spain); 5-nitro-1,3-benzodioxole (NBD) was acquired from TCI America; iProof DNA polymerase was from Bio-Rad (Hercules, CA, USA), whereas *Pfu*Ultra DNA polymerase and *Escherichia coli* XL1-Blue competent cells were from Agilent Technologies (Santa Clara, CA, USA). *Saccharomyces cerevisiae* strain BJ5465 was from LGC Promochem (Barcelona, Spain) and Zymoprep Yeast plasmid miniprep kit was from Zymo Research (Orange, CA, USA). The NucleoSpin Gel and PCR clean-up and NucleoSpin Plasmid kits were purchased from Macherey-Nagel (Düren, Germany) and the restriction enzymes BamHI and XhoI were from New England Biolabs (Hertfordshire, UK). Primers were synthesized by Metabion International AG (Steinkirhcen, Germany) (Table S1). Culture media were prepared as described elsewhere (Molina-Espeja *et al.*, 2014, 2016b). For microtiter growth and expression, selective expression medium was used, whereas for large-scale production rich expression medium was employed.

Analysis of *B*-factors and ΔΔ*G* values

The analysis of *B*-factors was performed applying the PyMOL Molecular Visualization System (version 1.3 Schrödinger, LLC) on the recently solved structure of PaDa-I mutant (unpublished material). The PoPMuSiC-2.1 algorithm was also used to search for amino acid substitutions that could enhance the thermal stability of PaDa-I using as threshold ΔΔ*G* values < −1 (Dehouck *et al.*, 2011). ΔΔ*G* values corresponding to single-site mutations were computed by the PoPMuSiC algorithm: $\Delta\Delta G(S_m,C_m;S_p,C_p) = \Delta G(S_m,C_m) - \Delta G(S_p,C_p)$, where C_m and C_p are the mutant and parent type conformations and S_m and S_p the mutant and parent type sequences, respectively (Gilis and Rooman, 2000). The output of PoPMuSiC that overlapped with the segments identified by PyMOL was chosen for experimental work.

Focused evolution (MORPHING)

From the *B*-factors and ΔΔ*G* analysis, five loops were selected for MORPHING. All of them were amplified and subjected to mutagenic PCR independently, while the rest of the sequence stretches were amplified by high-fidelity PCR (see below). Primers for amplification of the different segments were designed to generate between 30 and 50 bp of homology on both ends in order to promote *in vivo* splicing in such a way that they were reassembled and the linearized plasmid was repaired after transformation in yeast (Table S1). The online tool OligoAnalyzer 3.1 (http://eu.idtdna.com/calc/analyzer) was used to design the primers for each selected fragment of the protein.

Mutagenic PCR of targeted segments

Reaction mixtures were prepared in a final volume of 50 µl containing: 0.92 ng/µl DNA template, 90 nM direct primer, 90 nM reverse primer, 0.3 mM dNTPs (0.075 mM each), 3% (v/v) dimethyl sulfoxide (DMSO), 0.10–0.15 mM $MnCl_2$ (fixed depending on the fragment length; Table S2), 1.5 mM $MgCl_2$ and 0.05 U/µl *Taq* DNA polymerase. Mutagenic PCR was carried out on a gradient

thermocycler (Mycycler, Bio-Rad, USA) using the following program: 95°C for 2 min (1 cycle); 94°C for 45 s, 49.5–58.9°C (fixed between this range depending on the fragment length) for 45 s, 74°C for 1 min (28 cycles) and 74°C for 10 min (1 cycle).

High-fidelity PCR of non-mutated segments

Reaction mixtures were prepared in a final volume of 50 µl containing: 100 ng/µl DNA template, 10 µM direct primer, 10 µM reverse primer, 10 mM dNTPs (0.25 µM each), 3% (v/v) DMSO and 2.5 U/µl *Pfu*Ultra DNA polymerase. High-fidelity PCR was carried out on a gradient thermocycler with following program: 95°C for 2 min (1 cycle); 95°C for 45 s, 49.7–55.3°C (fixed between this range depending on the length of the fragment) for 45 s, 72°C for 1 min 30 s (30 cycles) and 72°C for 10 min (1 cycle).

Additionally, 2 µg of the shuttle vector pJRoC30 were linearized with 0.5 µl BamHI and XhoI (20 U/µl), 2 µl BSA 10 mg/ml, 2 µl NE Buffer 3 (10x) and $_{dd}H_2O$ up to 20 µl. Both linearized vector and PCR products were cleaned, concentrated and loaded into a low melting point preparative agarose gel and purified using the NucleoSpin Gel and PCR clean-up. The gene was reassembled *in vivo* and recombined by transformation in *S. cerevisiae* cells using the Yeast transformation kit. The DNA transformation mixture contained the linearized plasmid (200 ng) mixed with the corresponding mutagenized/non-mutagenized regions obtained by PCR (400 ng each). Transformed cells were plated on SC dropout plates and incubated at 30°C for 72 h. Individual clones were picked in sterile 96-well plates containing selective expression medium and mutant libraries were handled as described elsewhere (Molina-Espeja *et al.*, 2016b).

Combinatorial saturation mutagenesis

The C6-D12 mutant from the MORPHING library at Loop 11 was used as a template to explore positions 120 and 320 by CSM (Fig. 1, Table S2). To reduce codon redundancy and screening effort, a mixture of primers with NDT (N = A/T/C/G, D = no C), VHG (V = no T, H = no G) and TGG codons at the targeted position was used (Kille *et al.*, 2012) (Table S1). As aforementioned, primers with overlapping regions of ~40 bp on both ends of each fragment were designed to guarantee *in vivo* splicing with the linearized plasmid. Three PCRs were carried out in a final volume of 50 µl containing: 10 ng DNA template, 0.5 µM direct primer, 0.5 µM reverse primer, 0.8 mM dNTPs (0.2 mM each), 3% (v/v) DMSO, 0.10 mM $MnCl_2$ and 0.02 U/µl iProof DNA polymerase. The PCRs were run in a gradient thermocycler with the following program: 98°C for 30 s (1 cycle); 98°C for 10 s, 50.8–65.6°C (fixed between this range depending on the fragment length) for 30 s, 72°C for 30 s (30 cycles) and 72°C for 10 min (1 cycle). The three PCR products were cleaned, concentrated and loaded into a low melting point preparative agarose gel and purified using the NucleoSpin Gel and PCR clean-up. Of note, 200 ng of each fragment were mixed with 200 ng of the linearized vector and transformed in *S. cerevisiae* using the Yeast transformation kit for *in vivo* gene reassembly and cloning. As in the case of the MORPHING libraries, transformed cells were plated on SC dropout plates and incubated at 30°C for 72 h. Individual clones were picked and the mutant library was handled as described above.

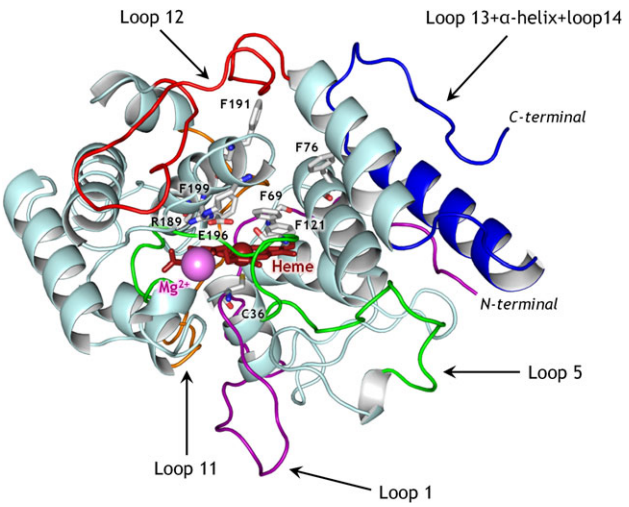

Fig. 1 Loops subjected to focused evolution in UPO (PaDa-I variant). Purple (Loop 1); green (Loop 5), orange (Loop 11), red (Loop 12) and blue cartoon (Loop 13 + α-helix + Loop 14). Non-mutagenized regions are shown as pale cyan cartoon. Phe residues delimiting the active site, the Cys36 axial ligand and the acid-base pair Arg189-Glu196 are depicted as gray sticks. The heme group is represented as dark red sticks, the heme Fe^{3+} ion as dark red sphere and the structural Mg^{2+} as pink sphere. See also Table S2.

High-throughput screening assays

All high-throughput screening (HTS) work was performed with the aid of a liquid handler robotic station Freedom EVO (Tecan, Switzerland) coupled to a pipetting robot (Multidrop Combi Reagent Dispenser, Thermo Scientific) and a plate reader (SPECTRAMax Plus 384, Molecular Devices). HTS assays for peroxidative activity (with ABTS) and peroxygenative activity (with NBD) were carried out and the P:p ratio was estimated as described elsewhere (Molina-Espeja *et al.*, 2014). HTS thermostability assay was performed as reported before with minor modifications (García-Ruiz *et al.*, 2010). Supernatants from microtiter plates were incubated in a thermocycler for 10 min at 70°C (temperature at which PaDa-I retains ~30% of its initial activity). Afterwards, samples were removed, cooled down for 10 min on ice and incubated 5 min at room temperature. The final values of thermostability came from the ratio of residual activity (after incubation) to initial activity (at room temperature) with NBD as substrate and normalized *vs.* the parental type.

With these HTS assays, five MORPHING libraries (~600 clones each) and one CSM library (1450 clones) were explored (~4500 clones in total). To rule out false positives, two consecutive re-screenings were carried out as previously reported (Molina-Espeja *et al.*, 2014).

P:p ratio and thermostability (T_{50} and $t_{1/2}$)

Single colonies of best clones were produced in larger scale format (100-ml flask) as described elsewhere (Molina-Espeja *et al.*, 2014) and characterized in terms of P:p ratio and thermostability. Activities with ABTS (peroxidative activity) were determined by triplicate by adding 180 µl of ABTS reaction mixture (100 mM sodium citrate–phosphate pH 4.4 with 0.3 mM ABTS and 2 mM H_2O_2) to 20 µl of supernatant with an appropriate dilution to give rise to a linear response in kinetic mode. Total activities with NBD (peroxygenase activity) were measured by triplicate by adding 180 µl of NBD reaction mixture (100 mM potassium phosphate buffer pH 7.0 with 1 mM NBD -15% final concentration of acetonitrile- and 1 mM H_2O_2) to 20 µl of supernatant with an appropriate dilution to give rise to a linear response in kinetic mode. Reactions were carried out by triplicate for each substrate concentration and substrate

conversion was followed by measuring the absorption at 418 nm for ABTS (ε_{418} = 36 000 M^{-1} cm^{-1}) and 425 for NBD (ε_{425} = 9700 M^{-1} cm^{-1}).

The T_{50} values (the temperature at which the enzyme retains 50% of its activity after 10 min incubation) were obtained as reported previously (Molina-Espeja *et al.*, 2014). Half-lives ($t_{1/2}$) of UPO variants were measured using 200 µl of crude extract with the appropriate dilution in such a way that 20 µl gave rise to a linear response in kinetic mode. Dilutions were done in 10 mM potassium phosphate buffer pH 7.0. First, the 200 µl samples were incubated over time at 63°C in a thermocycler. Then, 20 µl samples were taken every 5 min and transferred to a 96-well plate to measure NBD activity as described above. The $t_{1/2}$ were determined by the transition midpoint of the inactivation curve of the protein as a function of time, being defined as the time (in min) at which the enzyme keeps 50% of its activity at 63°C.

Mutant production, purification and characterization

The PaDa-I mutant was produced in large scale and purified as described elsewhere (Molina-Espeja *et al.*, 2014). The QuiGon and WinDu variants were produced and purified as PaDa-I mutant, with minor modifications: the culture supernatant (~1 L) was first concentrated to ~200 ml using a Pellicon tangential ultrafiltration system (10 kDa cut-off membrane; Millipore, MA, USA), followed by dialysis against 20 mM sodium citrate buffer pH 3.3 (Buffer A) and concentration to a final volume of ~20 ml using an Amicon stirred ultrafiltration cell (10 kDa cut-off membrane; Millipore). The sample was filtered and loaded to two cation-exchange HiTrap SP FF columns in a row connected to an ÄKTA purifier chromatography system (both from GE Healthcare, UK). The proteins were eluted with a linear gradient from 0% to 40% of Buffer B (20 mM sodium citrate buffer pH 3.3 1 M NaCl) for 60 min at a flow rate of 1 ml/min. The fractions with UPO activity toward ABTS were pooled, dialyzed against 20 mM Tris-HCl buffer pH 7.8 and loaded into a BioSuite Q anion-exchange column (Waters, MA, USA) connected to an ÄKTA purifier system. The proteins were eluted with a linear gradient from 0% to 20% of buffer 20 mM Tris-HCl buffer pH 7.8 1 M NaCl for 40 min at a flow rate of 1 ml/min. The fractions with UPO activity toward ABTS were collected, dialyzed against 10 mM potassium phosphate buffer pH 7.0 and concentrated using 3 kDa cut-off Amicon ultrafiltration units (Millipore). Samples of pure enzyme were stored at 4°C.

Initial turnover rates

Turnover rates were determined using saturated concentrations for each substrate tested (0.3 mM for ABTS, 2 mM for DMP, 1 mM for NBD and 25 mM for veratryl alcohol). Reactions were performed by triplicate and substrate conversion was followed by measuring the absorption at 418 nm for ABTS (ε_{418} = 36 000 M^{-1} cm^{-1}), 469 nm for DMP (ε_{469} = 27 500 M^{-1} cm^{-1}), 425 for NBD (ε_{425} = 9700 M^{-1} cm^{-1}) and 310 nm for veratryl alcohol (ε_{310} = 9300 M^{-1} cm^{-1}). ABTS turnover rates were estimated in 100 mM sodium citrate–phosphate buffer pH 4.4 containing 2 mM H_2O_2, and those for the rest of substrates in 100 mM potassium phosphate buffer pH 7.0 containing 1 mM H_2O_2 (NBD) or 2 mM H_2O_2 (DMP and veratryl alcohol).

Kinetic parameters

Kinetics were assayed with increasing substrate concentrations and fitted to a Michaelis–Menten model (steady-state enzyme kinetics) using as template a hyperbolic, single rectangular, two parameters mode (SigmaPlot software, v. 10.0). The catalytic efficiency (k_{cat}/K_m) was obtained plotting turnover rate (s^{-1}) *vs.* substrate concentration (mM) and fitting the data to a modified hyperbola with function $f(x) = (ax)/(1+bx)$, where a is catalytic efficiency and b is $1/K_m$. Kinetics for ABTS were performed in 100 mM sodium citrate–phosphate pH 4.4 containing 2 mM H_2O_2. Kinetics for NBD were done in 100 mM potassium phosphate buffer pH 7.0 containing 1 mM H_2O_2. Reactions were carried out by triplicate for each substrate concentration and substrate conversion was followed by measuring the absorption at 418 nm for ABTS (ε_{418} = 36 000 M^{-1} cm^{-1}) and 425 for NBD (ε_{425} = 9700 M^{-1} cm^{-1}).

DNA sequencing

Plasmid-containing mutant *upo1* genes were sequenced by GATC-Biotech (Germany). The samples were prepared with 5 µl of 100 ng/µl plasmid plus 5 µl of 5 µM of each primer (RMLN and RMLC, Table S1).

Results

Focused evolution

The starting point of this work is a UPO variant from a previous directed evolution campaign (Molina-Espeja *et al.*, 2014). This mutant (called PaDa-I) is the product of five rounds of random mutagenesis, DNA recombination and screening for secretion in *S. cerevisiae*. PaDa-I contains four mutations in the signal peptide (F[12]Y-A[14]V-R[15]G-A[21]D) that fostered secretion plus five mutations in the mature protein (V57A-L67F-V75I-I248V-F311L) that enhanced activity, secretion and stability.

Given that the catalytic sites for peroxidative activity in many ligninolytic peroxidases are both located at the heme access channel and at the protein surface—through an LRET from surface radical-forming residues to the heme—we inspected surface loops in the PaDa-I crystal structure searching for regions that fulfill a criteria established by the analysis of *B*-factors and the $\Delta\Delta G$ values. Computational calculations recognized five segments as suitable targets for focused evolution to modify the P:p ratio and/or enhance thermostability: Glu1-Pro35 (Loop 1), Gly103-Asp131 (Loop 5), Ser226-Gly243 (Loop 11), Gln254-Thr276 (Loop 12) and Tyr293-Arg327 (Loop 13 + Loop 14) (Fig. 1). Loops 13 and 14 are connected by a 17-amino acid α-helix (Val298-Gly314) (~50 bp), being that the length required for *in vivo* recombination in yeast, and thus precluding the possibility of treating both loops separately by MORPHING. Therefore, Loops 13 and 14 were gathered as just one single piece including this α-helix. MORPHING is a simple and robust method to introduce and recombine random mutations exclusively in small protein stretches while keeping the remaining regions of the protein without mutations (Gonzalez-Perez *et al.*, 2014). Mutational loads for MORPHING were adjusted so as to introduce between 1 and 3 mutations per segment (Table S2). Taking advantage of the high frequency of homologous recombination of *S. cerevisiae*, overlapping areas of ~40 bp were designed to promote reassembling of the whole gene and the *in vivo* cloning in just one single transformation step into yeast. Accordingly, each segment was independently subjected to MORPHING giving rise to the corresponding five mutant libraries. In total, the five selected regions comprised 141 amino acids, which correspond to 43% of the total protein sequence. Mutant libraries were screened in terms of thermostability and the P:p ratio (see Methods section for details).

The best mutant of the screening for thermal stability, the C6-D12 variant, was obtained from the MORPHING library in Loop 11. C6-D12 carried only the mutation S226G (Table I), which led to the retention of 52% of its initial activity after incubation for 5 min at 63°C along with a rise of ~2°C in the T_{50} compared to PaDa-I (Table II, Fig. 2). Moreover, MORPHING in Loop 5 resulted in two variants—B7-A11 and B7-C8—with a ~2-fold increase in the P:p ratio with respect to the parental type (Table 2). Interestingly, these two variants incorporated a mutation at position 120 (T120A, Table I), which was already identified as a hotspot for increasing the P:p ratio—but with T120P substitution—during the previous directed UPO evolution for secretion in *S. cerevisiae* (3F10 mutant; Molina-Espeja *et al.*, 2014). As observed for the 3F10 variant, such improvement of the P:p ratio in B7-A11 and B7-C8 was at the expense of a dramatic decrease in thermostability (with a drop in the T_{50} of ~7°C, Table II, Fig. 2). Unexpectedly, DNA polymerase failed during high-fidelity amplification, including two extra substitution (plus one silent mutation) in these two variants: at the signal leader K[2]N/T—this mutation only affected secretion irrespective of the mutant—and in the mature protein (T320A in the B7-A11 variant, Table I). As the latter substitution might be involved in the modification of the P:p ratio, we decided to explore all the possible combinations and synergies between positions 120 and 320 while trying to recover the lost stability. Thus, we performed CSM on such positions using as template the thermostable C6-D12 variant. From this library, five improved mutants—17B12 (T120P, S226G, T320R), 19F2 (T120P, S226G, T320P), 13B3 (T120P, S226G, T320K), QuiGon (T120V, S226G, T320R) and WinDu (T120V, S226G, T320N)—were selected (new mutations are underlined). It is worth noting that amino acid mutations at each of the targeted saturated positions were in all the cases the result of double or triple nucleotide substitutions so that they could not be achieved by conventional mutagenic PCR (Table I). All triple mutants showed a ~4-fold improvement in the P:p ratio compared to that of PaDa-I (Table II). More significantly, thanks to the harbored S226G stabilizing mutation, thermostability was partially recovered (with enhancements in the T_{50} of ~3°C, except for the case of the 13B3 mutant with the T320K mutation that seems to be highly detrimental for the stability).

Kinetic characterization

From the set of triple variants, QuiGon and WinDu mutants were chosen for further characterization as their P:p ratio satisfied us while their $t_{1/2}$ were slightly higher than that of their mutant counterparts (Table II, Fig. 2). They were produced, purified to homogeneity (with Reinheitszahl value [R_Z] [A_{418}/A_{280}] ~2) and their initial turnover rates assessed with peroxygenative and peroxidative

Table I. Mutations of UPO variants

Mutant	Mutagenesis strategy	Nucleotide mutations	Amino acid mutations
C6-D12	MORPHING in Loop 11	$_{676}$AGC/GGC$_{678}$	S226G
B7-A11	MORPHING in Loop 5	$_{[4]}$AAA/CAA$_{[6]}$[a], $_{358}$ACC/GCC$_{360}$, $_{958}$ACC/GCC$_{960}$[a]	K[2]N[a], T120A, T320A[a]
B7-C8	MORPHING in Loop 5	$_{[4]}$AAA/ACA$_{[6]}$[a], $_{317}$CCA/CCG$_{319}$[a], $_{358}$ACC/GCC$_{360}$	K[2]T[a], P106P[a], T120A
17B12	CSM 120 + 320[b]	$_{358}$ACC/CCG$_{360}$, $_{676}$AGC/GGC$_{678}$, $_{958}$ACC/CGT$_{960}$	T120P, S226G, T320R
19F2	CSM 120 + 320[b]	$_{358}$ACC/CCG$_{360}$, $_{676}$AGC/GGC$_{678}$, $_{958}$ACC/CCG $_{960}$	T120P, S226G, T320P
13B3	CSM 120 + 320[b]	$_{358}$ACC/CCG$_{360}$, $_{676}$AGC/GGC$_{678}$, $_{958}$ACC/AAG$_{960}$	T120P, S226G, T320K
QuiGon	CSM 120 + 320[b]	$_{358}$ACC/GTG$_{360}$, $_{676}$AGC/GGC$_{678}$, $_{958}$ACC/CGT$_{960}$	T120V, S226G, T320R
WinDu	CSM 120 + 320[b]	$_{358}$ACC/GTG$_{360}$, $_{676}$AGC/GGC$_{678}$, $_{958}$ACC/AAT$_{960}$	T120V, S226G, T320N

[a]Mutations incorporated due to a DNA polymerase error during PCR amplification.
[b]CSM 120+320: CSM at positions 120 and 320.
Nucleotide mutations within corresponding codons are underlined. Numbers between brackets indicate nucleotide and amino acid positions in the signal peptide.

Table II. Biochemical characterization of UPO variants

Mutant	Mutagenesis strategy	Total activity (U/l)[c]		P:p ratio (NBD/ABTS)	Improvement of P:p ratio *vs.* PaDa-I (in fold)	Thermal stability	
		ABTS	NBD			Residual activity after 5 min (%)[d]	T_{50} (°C)
PaDa-I	–	4611 ± 115	1484 ±114	0.32	1.0	45	58.3
sp*3F10[a]	–	1688 ± 105	2073 ± 140	1.23	3.8	13	50.0
C6-D12	MORPHING in Loop 11	3601 ± 152	1389 ± 132	0.39	1.2	52	60.2
B7-A11	MORPHING in Loop 5	1895 ± 50	1261 ± 116	0.66	2.1	4	51.8
B7-C8	MORPHING in Loop 5	2614 ± 55	1665 ± 72	0.64	2.0	2	50.9
17B12	CSM 120+320[b]	2118 ± 100	2573 ± 93	1.21	3.8	13	54.3
19F2	CSM 120+320[b]	1492 ± 45	1952 ± 38	1.31	4.1	14	53.3
13B3	CSM 120+320[b]	1316 ± 67	1750 ± 98	1.33	4.2	9	50.3
QuiGon	CSM 120+320[b]	2031 ± 47	2596 ± 90	1.28	4.0	24	54.3
WinDu	CSM 120+320[b]	1130 ± 38	1336 ± 18	1.18	3.7	20	54.3

[a]sp*3F10 is formed by the mature protein of the 3F10 variant preceded by the evolved signal peptide (Molina-Espeja *et al.*, 2014).
[b]CSM at positions 120 and 320 using C6-D12 as template.
[c]From culture supernatants.
[d]Residual activity after 5 min determined at 63°C, see also Fig. 2.

substrates (Table III). The general tendency observed from crude supernatants was maintained, with a notable decrease of the initial rates for peroxidative substrates while conserving or even enhancing them for peroxygenative substrates. To make a more reliable analysis of the P:p ratio of the variants, we measured the kinetic parameters with the two substrates employed in the screening for peroxygenative (NBD) and peroxidative (ABTS) activity (Table IV). As expected, the k_{cat} followed a similar pattern with a P:p ratio improvement of up to 1.8-fold over parental type. The differences in terms of catalytic efficiency for ABTS were not so pronounced due to the increase of the affinity for such substrate in the mutant variants, whereas the k_{cat}/K_m for NBD was conserved or even improved in the case of WinDu variant.

Discussion

The association between computational algorithms and directed evolution is paving the way in designing and improving different enzyme traits (Kiss *et al.*, 2013; Mate *et al.*, 2016). In this study, we have performed focused directed evolution in five independent segments of UPO that included several surface loops covering a little less than half of the total protein sequence. This approach has proved to be useful to find point mutations that modify the P:p ratio of the enzyme albeit at the cost of jeopardizing thermostability. Conversely, the discovery of the S226G stabilizing mutation gave us the opportunity to explore in deeper detail the point mutations responsible for the modification in the P:p ratio while recovering part of the lost stability.

Mutations found in this work were mapped onto the recently solved crystal structure of PaDa-I mutant (with a resolution of ~1.2 Å, unpublished material). The stabilizing mutation S226G lies in Loop 11 at the protein surface and 12 Å far from the ferric ion of the heme group (Fig. 3A, Table S3). The change for a smaller amino acid may compress this region although we have no convincing explanation for the overall stabilizing effect provoked by this

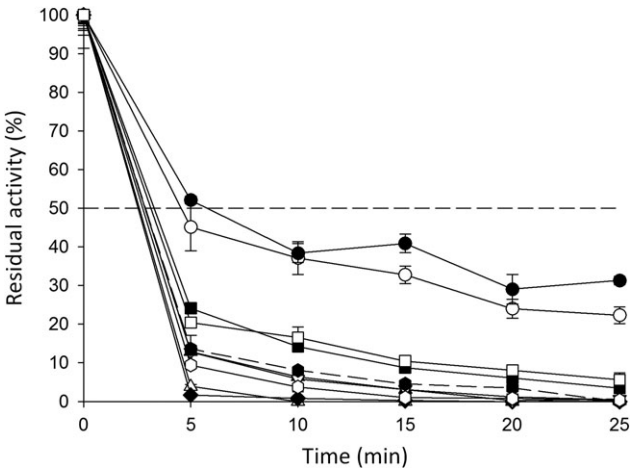

Fig. 2 $t_{1/2}$ of the different UPO variants at 63°C. White circles, PaDa-I parental type; black up triangles, sp*3F10 mutant; black circles, C6-D12 mutant; white up triangles, B7-A11 mutant; black diamonds, B7-C8 mutant; white down triangles, 17B12 mutant; black hexagons, 19F2 mutant; white hexagons, 13B3 mutant; black squares, QuiGon mutant and white squares, WinDu mutant. Each point represents the mean and standard deviation of three independent experiments.

Table III. Initial turnover rates of evolved variants

Variant	Initial turnover rate (μmol product·μmol enzyme^{-1}·s^{-1})			
	Peroxidative substrates		Peroxygenative substrates	
	ABTS	DMP	NBD	Veratryl alcohol
PaDa-I (parental type)	793 ± 20	110 ± 5	162 ± 10	71 ± 2
QuiGon	203 ± 7	79 ± 3	163 ± 8	77 ± 15
WinDu	232 ± 19	82 ± 4	186 ± 8	80 ± 4

Table IV. Kinetic parameters of evolved variants

Substrate	Kinetic constant	PaDa-I (parental type)	QuiGon	WinDu
ABTS	K_m (mM)	0.083 ± 0.006	0.043 ± 0.002	0.043 ± 0.003
	k_{cat} (s^{-1})	952 ± 27	380 ± 7	343 ± 7
	k_{cat}/K_m (mM^{-1} s^{-1})	11 424 ± 523	8891 ± 375	7982 ± 404
NBD	K_m (mM)	0.87 ± 0.01	0.49 ± 0.06	0.35 ± 0.03
	k_{cat} (s^{-1})	328 ± 8	192 ± 8	268 ± 5
	k_{cat}/K_m (mM^{-1} s^{-1})	406 ± 35	393 ± 36	748 ± 41

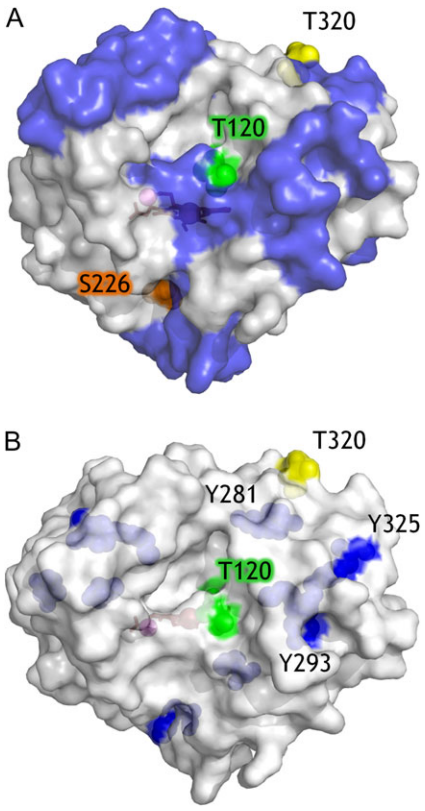

Fig. 3 PaDa-I crystal structure mapping the positions mutated in this study and potential radical-forming aromatic residues. (**A**) Amino acid positions mutated in this study. Thr120, Ser226 and Thr320 are highlighted in green, orange and yellow, respectively. Blue color indicates the regions subjected to MORPHING. (**B**) Thr120, Thr320 and potential radical-forming aromatic residues. Thr120 and Thr320 are highlighted in green and yellow, respectively. Tyr and Trp residues are shown painted in blue. Surface Tyr residues 281, 293 and 325 in the vicinity of Thr120 and Thr320 are labeled.

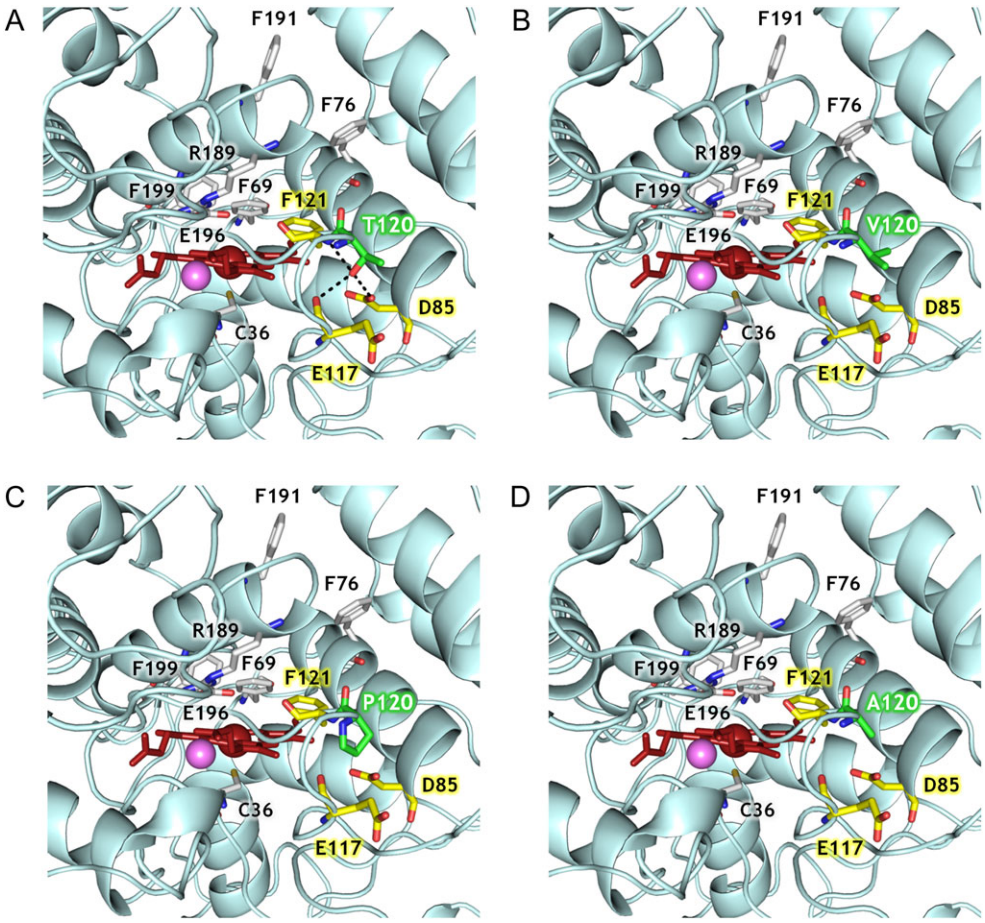

Fig. 4 Mutations found at positions 120. Thr (**A**), Val (**B**), Pro (**C**) and Ala (**D**) are shown as green sticks. The residues involved in hydrogen bond interactions with Thr120 (black dashes) are represented as yellow sticks. Phe residues delimiting the active site, the Cys36 axial ligand and the acid-base pair Arg189-Glu196 are depicted as gray sticks. The heme group is represented as dark red sticks, the heme Fe^{3+} ion as dark red sphere and the structural Mg^{2+} as pink sphere. See also Table S3.

substitution (i.e. we did not observe any change in the interactions with the surrounding residues). Thr320 is located at the surface of the protein in Loop 14, 25.8 Å away from the heme group and very close to the C-terminus (Fig. 3A, Table S3). According to our observations, no interactions with residues in the neighborhood are formed or interrupted after mutation regardless of the amino acid substitution, even though there is a clear relationship between this substitution (T320A/P/K/R/N, depending on the variant, Table 1) and the improved P:p ratio (Table 2). Thr120 is located in Loop 5 at the surface of the protein and 13.7 Å away from the heme (Fig. 3A, Table S3). This residue is adjacent to the structural Phe121 (one of the three Phe residues involved in substrate orientation in the heme (Piontek *et al.*, 2013)). A more detailed inspection of our model indicates that Thr120 establishes hydrogen bonds with Asp85, Glu117 and the structural Phe121. All these interactions are interrupted when the residue is mutated either to Ala, Pro or Val which may affect the P:p ratio but at the cost of sacrificing stability (Fig. 4A–D, Table S3).

In very recent experiments, we have found by focused evolution some key residues at the entrance of the heme channel that improve the total turnover numbers of UPO in the synthesis of human drug metabolites by reducing the unwanted peroxidative activity (unpublished material). More significantly, we already altered the P:p ratio to design an efficient UPO mutant for the selective synthesis of 1-naphthol (Molina-Espeja *et al.*, 2016b). One of the mutations responsible for this effect (G241D) was also placed at the entrance of the heme access channel which together with the results shown here indicates that peroxidative activity of UPO may be located in this site, but not exclusively. Indeed, when we applied computational analysis by Protein Energy Landscape Exploration and Quantum mechanics/Molecular mechanics to identify potential oxidation sites at the surface of UPO structure, we found Trp24 as the most favorable residue and further site-directed mutagenesis on Trp24 revealed its influence on both peroxidative and peroxygenative activities (Molina-Espeja *et al.*, 2016b). When considering these results all together, it seems plausible that Thr120 may be also involved in the catalysis by an LRET route to the heme, as described for other ligninolytic peroxidases. Certainly, it is well known that ligninolytic peroxidases show surface aromatic amino acids (Trp and/or Tyr) that are capable of forming active catalytic radicals involved in substrate oxidation. Surface Trp residues were first described as the origin of LRET in lignin peroxidase (LiP) from *Phanerochaete chrysosporium* (Doyle *et al.*, 1998) and versatile peroxidase (VP) from *Pleurotus eryngii* (Pérez-Boada *et al.*, 2005). In a similar way, contributions to substrate oxidation by a mixed tryptophanyl/tyrosyl radical have been recently shown in the dye-decolorizing peroxidase (DyP) from *Auricularia auricula-judae* (Linde *et al.*, 2015). Although Thr is not a radical-forming amino acid, it could participate in an LRET

through an electron transfer backbone which may vary in length and composition (e.g. the recent characterized LRET of DyP is formed by Trp377-Pro310-Arg309-Arg306-Ile305-His304-heme while the LRET of VP is Trp164-Leu165-heme).

From the eight potential radical-forming aromatic residues located at the UPO surface (Trp24, Tyr47, Tyr79, Tyr151, Tyr265, Tyr281, Tyr293 and Tyr325), only Tyr281, Tyr293 and Tyr325 are in the vicinity of the mutated Thr120 and Thr320 of this study (Fig. 3B). This suggests that any of these three Tyr residues might be the origin of an LRET from the surface to the heme and that any subtle modification in their surroundings, like those shown in this study, could influence the catalysis.

Future perspectives for a more drastic suppression of the non-desired peroxidative activity include saturation mutagenesis in aromatic residues (paying special attention to Tyr281, Tyr293 and Tyr325), along with the incorporation of other point mutations beneficial for the peroxygenative activity unveiled by neutral genetic drift (unpublished results).

Supplementary material

Supplementary material is available at *Protein Engineering, Design and Selection* online.

Acknowledgements

We truly thank Dr Julia Sanz from Instituto de Química-Física Rocasolano, IQFR-CSIC, for providing PaDa-I crystal structure.

Conflict of interest

The authors declare no competing financial interest.

Funding

This work was supported by the European Union [FP7-KBBE-2013-7-613549-INDOX, H2020-BBI-PPP-2015-2-720297-ENZOX2], the COST Action [CM1303 Systems Biocatalysis] and the Spanish Government [BIO2016-79106-R-Lignolution].

References

Damborsky,J. and Brezovsky,J. (2014) *Curr. Op. Chem. Biol.*, **19**, 8–16.

Dehouck,Y., Kwasigroch,J.M., Gilis,D. and Rooman,M. (2011) *BMC Bioinformatics*, **12**, 151.

Doyle,W.A., Blodig,W., Veitch,N.C., Piontek,K. and Smith,A.T. (1998) *Biochemistry*, **37**, 15097–15105.

García,E., Mate,D., Ballesteros,A., Martínez,A.T. and Alcalde,M. (2010) *Microb. Cell Fact.*, **9**, 17.

Gilis,D. and Rooman,M. (2000) *Protein Eng.*, **13**, 849–856.

Gonzalez-Perez,D., Molina-Espeja,P., Garcia-Ruiz,E. and Alcalde,M. (2014) *PLos ONE*, **9**, e90919.

Hofrichter,M. and Ullrich,R. (2006) *Appl. Microbiol. Biotechnol.*, **71**, 276–288.

Hofrichter,M., Ullrich,R., Pecyna,M.J., Liers,C. and Lundell,T. (2010) *Appl. Microbiol. Biotechnol.*, **87**, 871–897.

Hofrichter,M. and Ullrich,R. (2013) *Curr. Opin. Chem*, **19**, 116–125.

Hofrichter,M., Kellner,H., Pecyna,M.J. and Ullrich,R. (2015) Hrycay,E.G. and Bandiera,S.M. (eds), *Monooxygenase, Peroxidase and Peroxygenase Properties and Mechanisms of Cytochrome P450*, **851**. Advances in Experimental Medicine and Biology, USA, pp. 341–368.

Kille,S., Acevedo-Rocha,C.G., Parra,L.P., Zhang,Z.-G., Opperman,D.J., Reetz,M.T. and Acevedo,J.P. (2012) *ACS Synth. Biol.*, **2**, 83–92.

Kiss,G., Çelebi-Ölçüm,N., Moretti,R., Baker,D. and Houk,K.N. (2013) *Angew. Chem. Int. Ed.*, **52**, 5700–5725.

Linde,D., Pogni,R., Cañellas,M., *et al.* (2015) *Biochem. J.*, **466**, 253–262.

Mate,D.M., Gonzalez-Perez,D., Mateljak,I., Gomez de Santos,P., Vicente,AI and Alcalde,M. (2016) Brahmachari,G., Demain,A. and Adrio,J.L. (eds), *Biotechnology of Microbial Enzymes: Production, Biocatalysis and Industrial Applications*. Elsevier, Amsterdam, pp. 185–214.

Molina-Espeja,P., Garcia-Ruiz,E., Gonzalez-Perez,D., Ullrich,R., Hofrichter, M. and Alcalde,M. (2014) *Appl. Environ. Microb.*, **80**, 3496–3507.

Molina-Espeja,P., Ma,S., Mate,D.M., Ludwig,R. and Alcalde,M. (2015) *Enz. Microb. Tech.*, **73-74**, 29–23.

Molina-Espeja,P., Viña-Gonzalez,J., Gomez,B.J., Martin-Diaz,J., Garcia-Ruiz, E. and Alcalde,M. (2016a) *Biotechnol. Adv.*, **34**, 754–767.

Molina-Espeja,P., Cañellas,M., Plou,F.J., Hofrichter,M., Lucas,F., Guallar,V. and Alcalde,M. (2016b) *ChemBioChem.*, **17**, 341–349.

Nestl,B.M. and Hauer,B. (2014) *ACS Catal.*, **4**, 3201–3211.

Pérez-Boada,M., Ruiz-Dueñas,F.J., Pogni,R., Basosi,R., Choinowski,T., Martinez, M.J., Piontek,K. and Martinez,A.T. (2005) *J. Mol. Biol.*, **354**, 385–402.

Piontek,K., Strittmatter,E., Ullrich,R., Gröbe,G., Pecyna,M.J., Kluge,M., Scheibner,K., Hofrichter,M. and Plattner,D.A. (2013) *J. Biol. Chem.*, **288**, 34767–34776.

Ruiz-Dueñas,F.J., Morales,M., Garcia,E., Miki,Y., Martínez,M.J. and Martínez,A.T. (2009) *J. Exp. Bot.*, **60**, 441–452.

Ullrich,R., Nüske,J., Scheibner,K., Spantzel,J. and Hofrichter,M. (2004) *Appl. Environ. Microb.*, **70**, 4575–4581.

Verma,R., Schwaneberg,U. and Roccatano,D. (2012) *Comput. Struct. Biotechnol. J.*, **2**, e201209008.